Research Article | Vol. 24, No. 26 | 26 Dec 2016 | OPTICS EXPRESS 29459

Optics EXPRESS

Probe of symmetry reduction at domain walls by nonlinear Cherenkov measurement

BANG LIU,[1,2] YUANLIN ZHENG,[1,2] XIAOHUI ZHAO,[1,2] HAIGANG LIU,[1,2] AND XIANFENG CHEN[1,2,*]

[1]*State Key Laboratory of Advanced Optical Communication Systems and Networks, Department of Physics and Astronomy, Shanghai Jiao Tong University, Shanghai 200240, China*
[2]*Key Laboratory for Laser plasma (Ministry of Education), Collaborative Innovation Center of IFSA (CICIFSA), Shanghai Jiao Tong University, Shanghai 200240, China*
**Email: xfchen@sjtu.edu.cn*

Abstract: We report on the investigation of symmetrical properties of lithium niobate ($LiNbO_3$) domain walls utilizing the nonlinear Cherenkov radiation. Compared with $LiNbO_3$ bulk crystals, new nonzero elements of the $\chi^{(2)}$ tensor at domain walls are found by the Cherenkov second harmonic generation (CSHG) and Cherenkov sum frequency generation (CSFG) measurement. Experimentally, we demonstrate the symmetry reduction of domain walls, where the mirror inversion symmetry of $LiNbO_3$ lattice is broken while the threefold rotational symmetry still remains.

OCIS codes: (190.0190) Nonlinear optics; (190.4350) Nonlinear optics at surfaces; (190.2620) Harmonic generation and mixing.

References and links

1. R. W. Boyd, *Nonlinear Optics,* 3rd ed. (Elsevier Science, 2008).
2. S. M. Saltiel, D. N. Neshev, R. Fischer, W. Krolikowski, A. Arie, and Y. S. Kivshar, "Generation of second-harmonic conical waves via nonlinear bragg diffraction," Phys. Rev. Lett. **100**(10), 103902 (2008).
3. A. Shapira and A. Arie, "Phase-matched nonlinear diffraction," Opt. Lett. **36**(10), 1933–1935 (2011).
4. S. M. Saltiel, D. N. Neshev, W. Krolikowski, A. Arie, O. Bang, and Y. S. Kivshar, "Multiorder nonlinear diffraction in frequency doubling processes," Opt. Lett. **34**(6), 848–850 (2009).
5. H. Liu, J. Li, X. Zhao, Y. Zheng, and X. Chen, "Nonlinear Raman-Nath second harmonic generation with structured fundamental wave," Opt. Express **24**(14), 15666–15671 (2016).
6. Y. Zhang, Z. D. Gao, Z. Qi, S. N. Zhu, and N. B. Ming, "Nonlinear Cerenkov radiation in nonlinear photonic crystal waveguides," Phys. Rev. Lett. **100**(16), 163904 (2008).
7. X. Zhao, Y. Zheng, H. Ren, N. An, X. Deng, and X. Chen, "Nonlinear Cherenkov radiation at the interface of two different nonlinear media," Opt. Express **24**(12), 12825–12830 (2016).
8. D. H. Auston, K. P. Cheung, J. A. Valdmanis, and D. A. Kleinman, "Cherenkov radiation from femtosecond optical pulses in electro-optic media," Phys. Rev. Lett. **53**(16), 1555–1558 (1984).
9. J. Seidel, L. W. Martin, Q. He, Q. Zhan, Y.-H. Chu, A. Rother, M. E. Hawkridge, P. Maksymovych, P. Yu, M. Gajek, N. Balke, S. V. Kalinin, S. Gemming, F. Wang, G. Catalan, J. F. Scott, N. A. Spaldin, J. Orenstein, and R. Ramesh, "Conduction at domain walls in oxide multiferroics," Nat. Mater. **8**(3), 229–234 (2009).
10. G. Catalan, J. Seidel, R. Ramesh, and J. F. Scott, "Domain wall nanoelectronics," Rev. Mod. Phys. **84**(1), 119–156 (2012).
11. S. Lei, E. A. Eliseev, A. N. Morozovska, R. C. Haislmaier, T. T. A. Lummen, W. Cao, S. V. Kalinin, and V. Gopalan, "Origin of piezoelectric response under a biased scanning probe microscopy tip across a 180° ferroelectric domain wall," Phys. Rev. B **86**(13), 134115 (2012).
12. T. Kämpfe, P. Reichenbach, A. Haußmann, T. Woike, E. Soergel, and L. Eng, "Real-time three-dimensional profiling of ferroelectric domain walls," Appl. Phys. Lett. **107**(15), 152905 (2015).
13. Y. Sheng, V. Roppo, K. Kalinowski, and W. Krolikowski, "Role of a localized modulation of χ(2) in Čerenkov second-harmonic generation in nonlinear bulk medium," Opt. Lett. **37**(18), 3864–3866 (2012).
14. H. Ren, X. Deng, Y. Zheng, N. An, and X. Chen, "Enhanced nonlinear Cherenkov radiation on the crystal boundary," Opt. Lett. **38**(11), 1993–1995 (2013).
15. X. Deng and X. Chen, "Domain wall characterization in ferroelectrics by using localized nonlinearities," Opt. Express **18**(15), 15597–15602 (2010).
16. A. Fragemann, V. Pasiskevicius, and F. Laurell, "Second-order nonlinearities in the domain walls of periodically poled $KTiOPO_4$," Appl. Phys. Lett. **85**(3), 375 (2004).
17. X. Deng, H. Ren, Y. Zheng, K. Liu, and X. Chen, "Significantly enhanced second order nonlinearity in domain walls of ferroelectrics," https://arxiv.org/abs/1005.2925.

#278858 http://dx.doi.org/10.1364/OE.24.029459
Journal © 2016 Received 17 Oct 2016; revised 6 Dec 2016; accepted 7 Dec 2016; published 12 Dec 2016

Optics EXPRESS

18. Y. Sheng, A. Best, H. J. Butt, W. Krolikowski, A. Arie, and K. Koynov, "Three-dimensional ferroelectric domain visualization by Cerenkov-type second harmonic generation," Opt. Express **18**(16), 16539–16545 (2010).
19. T. Kämpfe, P. Reichenbach, M. Schroder, A. Haussmann, L. M. Eng, T. Woike, and E. Soergel, "Optical three-dimensional profiling of charged domain walls in ferroelectrics by Cherenkov second-harmonic generation," Phys. Rev. B **89**(3), 035314 (2014).
20. H. Ren, X. Deng, Y. Zheng, N. An, and X. Chen, "Nonlinear Cherenkov radiation in an anomalous dispersive medium," Phys. Rev. Lett. **108**(22), 223901 (2012).
21. X. Chen, P. Karpinski, V. Shvedov, K. Koynov, B. Wang, J. Trull, C. Cojocaru, W. Krolikowski, and Y. Sheng, "Ferroelectric domain engineering by focused infrared femtosecond pulses," Appl. Phys. Lett. **107**(14), 141102 (2015).
22. N. An, Y. Zheng, H. Ren, X. Deng, and X. Chen, "Conical second harmonic generation in one-dimension nonlinear photonic crystal," Appl. Phys. Lett. **102**(20), 201112 (2013).

1. Introduction

Periodically poled ferroelectrics are designed to achieve quasi-phase-matching proposed by Bloembergen in 1962 [1], which can significantly improve the efficiency in nonlinear frequency conversion. Over the past decades, periodically poled crystals such as $LiNbO_3$ (PPLN), $KTiOPO_4$ (PPKTP) and $LiTaO_3$ (PPLT) have been widely used in optical parameter processes and kinds of nonlinear optical phenomena are observed in these media, such as nonlinear Bragg diffraction [2, 3], nonlinear Raman-Nath diffraction [4, 5] as well as nonlinear Cherenkov radiation (NCR) [6–8]. Domain walls, the boundaries between positive and negative domains in ferroelectrics, reveal specific properties such as conductivity, mobility and symmetry different from the bulk medium and have a promising application in nanoscale functional devices [9, 10]. In recent years, much attention has been paid to the research on novel properties and applications of domain walls. And many detection and visualization methods have been developed to explore the inner structure of domain walls, mainly including optical imaging and scanning probe microscopy [10–12]. Nevertheless, the mechanism of enhanced nonlinear parametric processes in domain walls is still controversial [13, 14], and one convincing explanations attributes it to the new enhanced susceptibility tensor owing to the lattice distortion [15] and the localized internal electrical field [16], which directly demonstrates different symmetrical properties of domain walls [17].

Meanwhile, the nonlinear Cherenkov radiation (NCR) is a nondestructive nonlinear measurement with high precision in probing domain wall nonlinearities [15–19]. Analogous to the Cherenkov radiation emitted by relativistic charged particles, the nonlinear polarization (NP) which is driven by the fundamental wave (FW) generates the NCR when its phase velocity exceeds that of the harmonic wave (HW) in nonlinear media [20, 21]. Since the NCR generated by domain walls is much more significant than domain region owing to the confinement of NP, the structural and symmetrical properties of domain walls can be measured reliably and efficiently. In addition, this NCR measurement is much simpler and more achievable than other scanning probe microscopy techniques.

In this paper, to obtain the entire second-order susceptibility tensor of PPLN domain walls qualitatively and investigate the difference between domain walls and bulk medium, we detect the polarization of the CSHG and CSFG while changing the incident beam. And based on the new nonzero elements in the $\chi^{(2)}$ tensor, the symmetry properties of domain walls of PPLN are demonstrated, which may push forward the research on the inner structure and the susceptibility of domain walls.

2. Theoretical model

For second-order nonlinear processes in $LiNbO_3$, the NP can be expressed by the FW and the $\chi^{(2)}$ susceptibility tensor [1] in the form of:

Optics EXPRESS

$$\begin{bmatrix} P_x(\omega_3) \\ P_y(\omega_3) \\ P_z(\omega_3) \end{bmatrix} = 4\varepsilon_0 \begin{bmatrix} 0 & 0 & 0 & 0 & d_{31} & -d_{22} \\ -d_{22} & d_{22} & 0 & d_{31} & 0 & 0 \\ d_{31} & d_{31} & d_{33} & 0 & 0 & 0 \end{bmatrix} \begin{bmatrix} E_x(\omega_1)E_x(\omega_2) \\ E_y(\omega_1)E_y(\omega_2) \\ E_z(\omega_1)E_z(\omega_2) \\ E_y(\omega_1)E_z(\omega_2)+E_y(\omega_2)E_z(\omega_1) \\ E_x(\omega_1)E_z(\omega_2)+E_x(\omega_2)E_z(\omega_1) \\ E_x(\omega_1)E_y(\omega_2)+E_x(\omega_2)E_y(\omega_1) \end{bmatrix}. \quad (1)$$

Considering the process of NCR at domain walls, the probe of symmetry reduction can be observed by monitoring the emitted HW generated through CSHG and CSFG. Since the CSHG and CSFG carry the information of domain walls in the NCR processes, the $\chi^{(2)}$ tensor of domain walls can be fully determined by detecting their polarizations based on Eq. (1).

In our experiment, a mode-locked Nd:YAG laser (1064 nm) is employed as the FW source, which delivers 10.5-ns pulses with 5 mJ per pulse energy at a repetition of 1 kHz. The dimension of the z-cut periodically poled 5mol% MgO:$LiNbO_3$ sample (the optical axis is along the z direction) is $20\times4\times1\,\mathrm{mm}^3$ $(x\times y\times z)$. The poling period Λ is 30 μm and the duty radio is 45%. The domain walls of PPLN are parallel to the y-z plane. As shown in Fig. 1(a), the FW is divided into a p(parallel)-polarized wave and a s(senkrecht)-polarized wave by a polarized beam splitter. The polarization of the beams is adjusted by two half-wave plates at 1064 nm, respectively, and then focused to overlap spatially in PPLN by two separate lens. At last, a 532 nm polarizer is utilized to check the polarization of the generated HWs.

3. Experimental results

3.1 NCR perpendicular to the optical axis of PPLN

Experimentally, the normal incidence ω_1 in Fig. 1(a) was employed in the CSHG, and both ω_1 and ω_2 were for the CSFG.

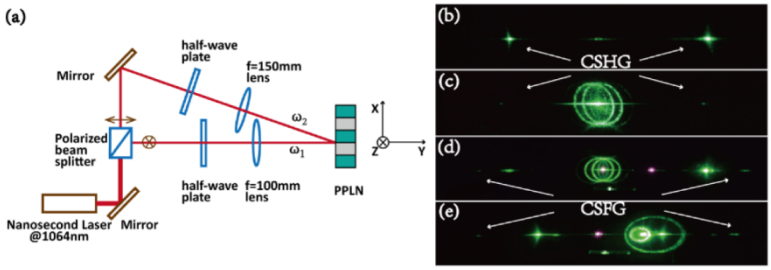

Fig. 1. (a) Schematic experimental setup. (b) The CSHG with the s-polarized normal incidence ω_1. (c) The CSHG with the p-polarized normal incidence ω_1. (d) The CSFG with the p-polarized normal incidence ω_1 and the s-polarized oblique incidence ω_2. (e) Exchange the polarization of the incident beams in (d).

In the CSHG process, when the FW was s-polarized, which means its electric component was E_z, the symmetrical spots were the CSHGs in Fig. 1(b). The spots in the middle were caused by the nonlinear Raman-Nath diffraction [5]. These Cherenkov spots were s-polarized when checked by a 532 nm polarizer, which means the HW had the electric component of $E_z(2\omega)$ and the NP wave had the component of $P_z(2\omega)$. Thus the effective value of d can be written as $d_{eff}=d_{33}$ in this NCR process. In addition, $E_x(2\omega)$ and $E_y(2\omega)$ had not been observed on the screen, so $d_{13}=d_{23}=0$ and $d_{33}\neq0$ in the susceptibility tensor of domain walls, corresponding to the ee-e phase match type.

Optics EXPRESS

For the p-polarized incidence, namely the electric component was E_x, the symmetrical Cherenkov spots were also p-polarized (see Fig. 1(c)). Considering the oblique outgoing beam, the HW possessed the components $E_x(2\omega)$ and $E_y(2\omega)$. Accordingly, $d_{eff} = d_{11}\sin\varphi - d_{21}\cos\varphi$ for oo-o phase match in this process, where φ is the azimuthal angle of the polarization of HW with respect to the positive x axis. Then $d_{11} \neq 0$ and $d_{21} \neq 0$ based on Eq. (1) whereas $d_{11} = 0$ in bulky $LiNbO_3$. However, d_{31} can't be determined since the NCR can't be stimulated in this oo-e anomalous dispersion circumstance, where the HW propagates faster than the NP for $n_e(532nm) < n_o(1064nm)$ in $LiNbO_3$ [20]. The conical pattern was generated by the scattering assisted phase-match process [22]. The spots in the center were due to the nonlinear Raman-Nath diffraction.

As to CSFG process, when the normal incident beam ω_1 was p-polarized and the oblique beam ω_2 was s-polarized, the marked outer pair of the CSFG spots in Fig. 1(d) was p-polarized and corresponded to the oe-o phase-match type. The effective coefficient $d_{eff} = d_{15}\sin\varphi - d_{25}\cos\varphi$. Considering the electric field of CSFG $E_z(\omega_3)$ had not been observed in the NCR normal dispersion condition, so d_{15}, $d_{25} \neq 0$ and $d_{35} = 0$. While ω_1 was s-polarized and ω_2 was p-polarized, the figure was demonstrated in Fig. 1(e). The marked outer pair of the p-polarized spots were CSFGs and belonged to the eo-o phase-match type. Thus $d_{eff} = -d_{14}\sin\varphi\cos\varphi_2 - d_{15}\sin\varphi\sin\varphi_2 + d_{24}\cos\varphi\cos\varphi_2 - d_{25}\sin\varphi\sin\varphi_2$, where φ_2 is the azimuthal angle of the polarization of the oblique FW with respect to the positive x axis. Since no $E_z(\omega_3)$ had been observed, we obtained $d_{34} = 0$.

Rotating the PPLN until its x axis was perpendicular to the platform as shown in Fig. 2(a), two pairs of the marked spots in the middle were CSFGs. While both ω_1 and ω_2 were p-polarized, the CSFG spots in Fig. 2(b) didn't contain the $E_x(\omega_3)$ when checked by a polarizer. Considering the normal incidence was $E_z(\omega_1)$ and the oblique incidence were $E_y(\omega_2)$ and $E_z(\omega_2)$, as we already had $d_{13} = 0$, the element $d_{14} = 0$ based on Eq. (1).

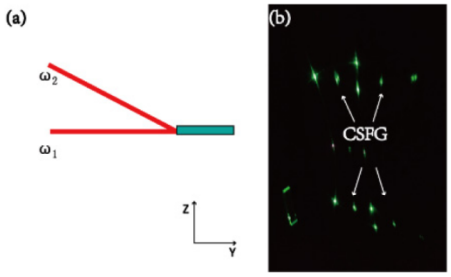

Fig. 2. (a) The CSFG schematic setup. (b) The CSFG pattern on the screen when both ω_1 and ω_2 were p-polarized.

3.2 NCR along the optical axis of PPLN

As shown in Fig. 3, the CSHG and CSFG patterns had been observed when FWs were along the z axis of PPLN.

Optics EXPRESS

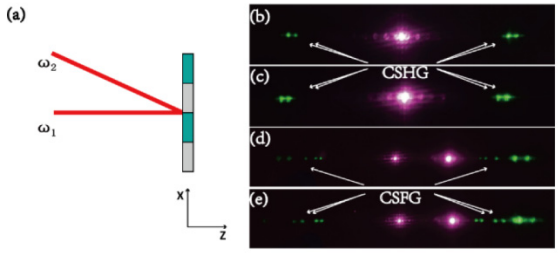

Fig. 3. (a) Schematic experimental setup. (b) The CSHG with the s-polarized normal incidence ω_1. (c) The CSHG with the p-polarized normal incidence ω_1. (d) The CSFG with the p-polarized normal incidence ω_1 and the s-polarized oblique incidence ω_2. (e) Exchange the polarization of the incident beams in (d).

As the ω_1 was p-polarized in CSHG, the outer pair of spots in Fig. 3(b) was s-polarized while the inner pair was p-polarized. For the inner pair, the HW possessed the components $E_x(2\omega)$ and $E_z(2\omega)$. So the coefficients $d_{eff1} = d_{21}$ and $d_{eff2} = -d_{11}\sin\theta + d_{31}\cos\theta$, respectively, where θ is the polar angle of the HW with respect to the positive z axis. So $d_{21} \neq 0$ and d_{11}, $d_{31} \neq 0$ based on Eq. (1), which belonged to the oo-o and oo-e* phase-match process, respectively. The notation e* means that there is an angle with respect to the axis z and it's a NCR process in normal dispersion. For the s-polarized incidence, two pairs of the CSHG were demonstrated on Fig. 3(c) and their polarization were the same as the last circumstance, where $d_{eff1} = d_{22}$ and $d_{eff2} = -d_{12}\cos\theta + d_{32}\sin\theta$, respectively. Therefore, d_{12}, d_{22} and $d_{32} \neq 0$ in the tensor.

Regarding the CSFG shown in Fig. 3(a), when ω_1 was p-polarized and ω_2 was s-polarized, the marked CSFG spots were p-polarized in Fig. 3(d) and $d_{eff} = -d_{16}\cos\theta + d_{36}\sin\theta$ in this oo-e* process. However, $E_x(\omega_3)$ and $E_z(\omega_3)$ had been detected but there was no $E_y(\omega_3)$. So based on Eq. (1), d_{16}, $d_{36} \neq 0$ and $d_{26} = 0$ in the matrix. Exchanging the polarization of ω_1 and ω_2, the inner pair of CSFG spots in Fig. 3(e) was p-polarized and the outer pair was s-polarized. Thus $d_{eff1} = d_{14}\cos\theta\sin\theta_2 - d_{16}\cos\theta\cos\theta_2 + d_{36}\sin\theta\cos\theta_2 \left(d_{34} = 0\right)$ and $d_{eff2} = -d_{24}\cos\theta_2 \left(d_{26} = 0\right)$, respectively, where θ_2 is the polar angle of ω_2 with respect to the positive z axis. Accordingly, the element $d_{24} \neq 0$.

4. Summary and discussion

The Cherenkov angles in the CSHG and CSFG processes are summarized in Table 1, which agrees well with the theoretical analysis.

Table 1. Cherenkov angles of the CSHG and CSFG in $LiNbO_3$ domain walls.

Incidence	Cherenkov type	Incident components	Outgoing components	Phase match type	Theoretical angles (degrees)	Experimental angles (degrees)
Perpendicular to optical axis	CSHG	Ez	Ez	ee-e	35.2	34.4
		Ex	Ex,Ey	oo-o	39.7	38.8
	CSFG	Ex&Ez	Ex,Ey	oe-o	54.9	55.1
		Ez&Ex,Ey	Ex,Ey	eo-o	54.8	55.1
Parallel to optical axis (e* means normal dispersion NCR)	CSHG	Ex or Ey	Ey	oo-o	39.7	38.7
		Ex or Ey	Ex,Ez	oo-e*	37.9	37.3
	CSFG	Ex&Ey	Ex,Ez	oo-e*	42.7	43.3
		Ey&Ex,Ez	Ex,Ez	oe-e	42.9	43.3
		Ey&Ex,Ez	Ey	oe-o	45.1	45.6

Optics EXPRESS

To summarize, we get the second-order susceptibility tensor of lithium niobate domain walls, expressed as

$$d_{ij}=\begin{bmatrix} \underline{\underline{d_{11}}} & \underline{\underline{d_{12}}} & \underline{0} & 0 & d_{31} & -d_{22} \\ -d_{22} & d_{22} & \underline{0} & d_{31} & \underline{\underline{d_{24}}} & 0 \\ d_{31} & d_{31} & d_{33} & \underline{0} & \underline{0} & \underline{\underline{d_{36}}} \end{bmatrix}. \tag{2}$$

For lithium niobate, the 3 × 3 × 3 tensor of $\chi^{(2)}_{ijk}$ transforms into a 3 × 9 matrix if we merge the last two indices and denote each element by its Cartesian indices [1], which has the form of:

$$\chi^{(2)}=\begin{bmatrix} 0 & 0 & \underline{0} & 0 & 0 & XZX & XXZ & \overline{YYY} & \overline{YYY} \\ \overline{YYY} & YYY & \underline{0} & XXZ & XZX & 0 & 0 & 0 & 0 \\ ZXX & ZXX & ZZZ & \underline{0} & \underline{0} & \underline{0} & \underline{0} & 0 & 0 \end{bmatrix}. \tag{3}$$

In point group theory, the lattice of lithium niobate belongs to C_{3v} point group and obeys threefold rotational symmetry and mirror inversion symmetry, where the rotational axis is the z axis and the mirror plane is yz-plane perpendicular to the x axis, respectively. In detail, threefold rotational symmetry means the lattice of the crystal is consistent with itself under $\frac{2}{3}\pi$ and $\frac{4}{3}\pi$ rotation around the z axis.

In Eq. (3), the underlined zeros and other nonzero elements are determined by the threefold rotational symmetry of $LiNbO_3$, and other zeros are determined by the mirror inversion symmetry with respect to yz-plane. Applying the Kleinman symmetry and contracted notion [1], we get the 3 × 6 matrix in Eq. (1). Comparing the matrix of bulk $LiNbO_3$ in Eq. (1) with PPLN domain walls in Eq. (2), the double underlined elements become nonzero while the underlined zeros and other nonzero elements remain. Therefore, we can draw a conclusion that the mirror inversion symmetry is violated and the threefold rotational symmetry is retained. And we can conclude there is a symmetry reduction at the PPLN domain walls.

5. Conclusion

In this work, the $\chi^{(2)}$ tensor of PPLN domain walls are full determined by detecting the polarization of CSHG and CSFG. The elements d_{11} and d_{12} in the $\chi^{(2)}$ matrix are found to contribute to the CSHG, and in situ, d_{25} and d_{36} have contribution to the CSFG, which are all zero in $LiNbO_3$ bulk medium. In conclusion, we demonstrate that the mirror symmetry in PPLN domain walls is broken, while the threefold rotational symmetry still remains during the periodically poling process. Moreover, this Cherenkov measurement may find its application in exploring the inner structure and the susceptibility properties of domain walls in other ferroelectrics.

Funding

National Natural Science Foundation of China (NSFC) (61235009, 61205110, 61505189); the Foundation for Development of Science and Technology of Shanghai (13JC1408300); the Innovative Foundation of Laser Fusion Research Center; the Presidential Foundation of the China Academy of Engineering Physics (201501023).